3D printing of layered ceramic/carbon fiber composite with improved toughness

Sun, Jinxing; Yu, Shixiang; Wade-Zhu, James; Chen, Xiaoteng; Binner, Jon; Bai, Jiaming

DOI:
10.1016/j.addma.2021.102543

Document Version
Peer reviewed version

Citation for published version (Harvard):
Sun, J, Yu, S, Wade-Zhu, J, Chen, X, Binner, J & Bai, J 2022, '3D printing of layered ceramic/carbon fiber composite with improved toughness', *Additive Manufacturing*, vol. 50, 102543. https://doi.org/10.1016/j.addma.2021.102543

3D printing of layered ceramic/carbon fiber composite with improved toughness

Jinxing Sun[a,b], Shixiang Yu[a], Jinsi Yuan[a], Haowen Liang[a], Jon Binner[b], Jiaming Bai[a*]

a. Shenzhen Key Laboratory for Additive Manufacturing of High-performance Materials，Department of Mechanical and Energy Engineering, Southern University of Science and Technology, Shenzhen, 518055, China

b. School of Metallurgy and Materials, University of Birmingham, B15 2TT, UK

* Corresponding Author: baijm@sustech.edu.cn (J. Bai)

Abstract

Strong and tough materials are required for many industrial applications, however these properties tend to be mutually exclusive in many man-made materials. Natural materials like nacre, however, simultaneously offer both high strength and toughness. In this work, nacre-inspired composites with layered architectures have been fabricated using digital light processing (DLP) of porous ceramic structures combined with the *in-situ* polymerization of methyl methacrylate (MMA). The resulting binary layered ceramic-polymer composites exhibit high strength and toughness. In addition, the introduction of carbon fibre bundles into the polymer layer significantly improved the mechanical properties of the composites even further; these ternary composites achieved an excellent combination of high strength (611.4 ± 46.7 MPa), fracture toughness (14.87 ± 0.83 MPa $m^{1/2}$) and work of fracture (6597.2 ± 99.3 J/m^2). Such

fracture-resistant behaviour can be attributed to toughening mechanisms of crack deflection, lamellae and fibre 'pull-out', polymer inelastic deformation and interfacial debonding. This study paves a new way to realize the fabrication of bioinspired ceramic composites with improved mechanical properties.

1. Introduction

The inherent brittleness of monolithic ceramics greatly constrains their usefulness for a wide range of applications because they have relatively immobile dislocations and consequently an almost total absence of plasticity during fracture processes [1][2]. Therefore, the development of ceramic matrix composites with improved toughness has been an important goal for industrial and academic communities. There are various biological materials in nature that inherently possess a unique combination between high strength and toughness, as they need to provide resistance to penetration against external impact [3]. Nacre, for example, consisting of 95% brittle phase and 5% ductile organic phase, is a natural composite with a layered structure in which the brittle phase is bonded together with ductile organic layers to form a "brick and mortar" architecture. It has been demonstrated that this architecture is the origin of nacre's high strength and toughness [4][5][6] with its fracture toughness being three to nine times higher than that of its constituents individually [7][8].

Nacre-inspired composites have been fabricated through a variety of approaches to date, including electrophoretic deposition [9], sputtering [10] and sol-gel processes [11].

However, these methods are all limited to the formation of thin multilayers, which constrain the fabrication of bulk components. Freeze casting, also known as ice-templating, has been shown to be one of the most effective alternative approaches and has been used to produce bioinspired bulk composites [12]. In this process, an aqueous ceramic slurry is frozen and then the ice is removed leaving a dendritic structure that forms a layered scaffold; both the ceramic loading and cooling rate play important roles in controlling the ceramic lamellar thickness. Bulk layered ceramic composites are then obtained by infiltrating the scaffold with a second phase, such as a polymer and/or a metal. For example, Bai et al. used a bidirectional freezing technique to fabricate lamellar hydroxyapatite scaffolds and infiltrated them with poly(methyl methacrylate) (PMMA) to produce HA/PMMA binary composite with exceptional combinations of strength (~100 MPa), elastic stiffness (~20 GPa) and work of fracture (265-2075 J m^{-2}) [13]. Munch et al. also infiltrated PMMA into freeze-cast alumina scaffolds to produce nacre-like Al_2O_3/PMMA composites with high ceramic content [14]. In order to improve the interface bonding, they firstly modified alumina scaffolds; the resultant composites displayed greatly improved flexural strength and fracture toughness.

Although freeze casting techniques combined with infiltration have been shown to be successful in the fabrication of nacre-like composites, this technique is cumbersome and has challenges in terms of precisely controlling the scaffold architecture. Moreover, the freeze cast scaffold size is limited by the mould, further limiting the technique's potential to make physically large composites [12][15]. Additive manufacturing, also

known as 3D printing, provides a simple, yet versatile route to fabricate ceramic parts with customized and complex architectures [16]. The fabrication of bioinspired, layered ceramic scaffolds via 3D printing offers particularly significant benefits compared to freeze casting, viz. ease of fabrication and customized geometry.

In this study, digital light processing (DLP)-based 3D printing technology was used to fabricate layered zirconia scaffolds. The layered composite was subsequently obtained by infiltrating PMMA into the as-sintered scaffold. In addition, scaffolds with and without embedded carbon fibre bundles were prepared prior to infiltration, the idea being to greatly mitigate the fibre damage that typically occurs in fibre-reinforced ceramic matrix composites that are made via high temperature sintering. The incorporation of carbon fibre into the PMMA was expected to further improve the mechanical properties of the composites, particularly the flexural strength, fracture toughness and work of fracture.

2. Experimental methodology

2.1 Materials

The following materials were used in this study as received: as-prepared zirconia slurry (see the process of slurry preparation in **Supporting information**), ethanol (Sigma-Aldrich GmbH, Germany), γ-methacryloxypropyl trimethoxy silane (γ-MPS, KH-570, Sigma-Aldrich GmbH, Germany) as silane coupling agent, methyl methacrylate (MMA, Sigma-Aldrich GmbH, Germany), azobisisobutyronitrile initiator (AIBN, Sigma-Aldrich GmbH, Germany), sulphuric acid (H_2SO_4, purity. 95.0-97.0, Sigma-Aldrich

GmbH, Germany), hydrogen peroxide (H_2O_2, 35 wt.% solution in water, Sigma-Aldrich GmbH, Germany), acetone (≥99.5%, ACS reagent, Merck, China), and the commercial carbon fibre bundle (SYT49S-12K, Zhongfu Shenying Carbon Fibre Co., Ltd, Jiangsu, China). The density of the carbon fibre bundle was 1.78 g/cm^3, the tensile strength and elastic modulus were 4900 MPa and 230 GPa, respectively.

2.2 Design and fabrication of layered zirconia scaffold

Fig. 1 shows a schematic illustration for producing the layered scaffold models with a ceramic content of 60, 65, 70 and 75 vol.%. The latter were designed using Materialise Majic software (Materialise software, Leuven, Belgium), as shown in **Fig. 1C**. The ceramic content could be controlled by changing the lamellae thickness (0.8, 1.0, 1.2, and 1.5 mm respectively); the gap between adjacent lamellae being fixed at 0.7 mm. In order to control the scaffold thickness for different specimens, the number of ceramic lamellae was varied. All zirconia green bodies were fabricated using a homemade DLP 3D printer, subsequently, they were debound and sintered in a furnace; the details can be found in the sample preparation process in the support information.

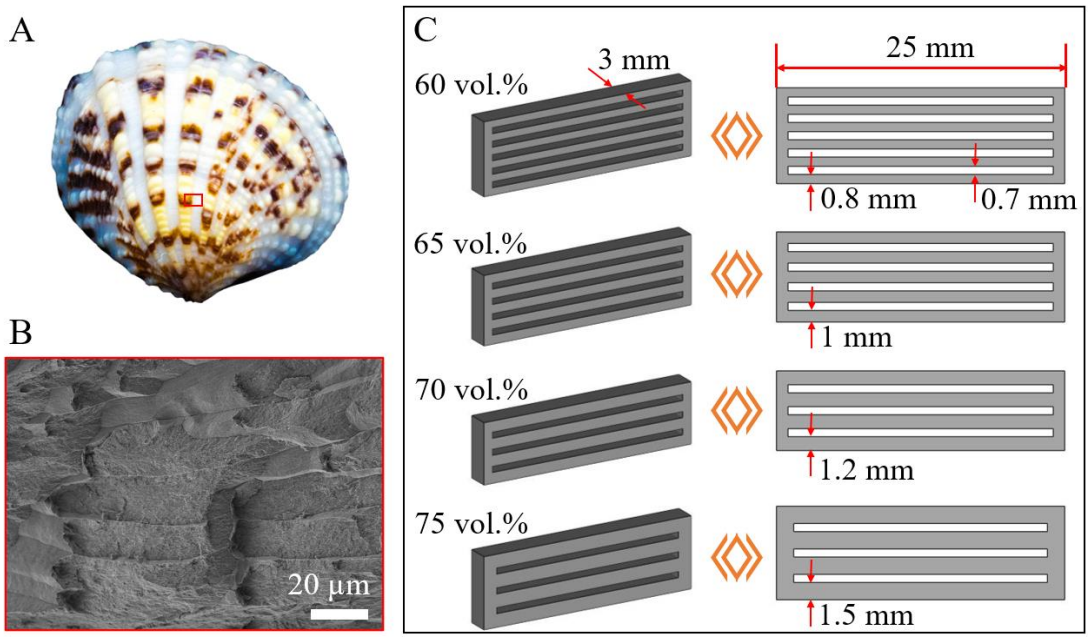

Fig. 1. Design principle of the nacre-inspired layered scaffold. (A) Representative photograph of nacre. (B) SEM image of nacre exhibiting a layered architecture consisting of an inorganic phase and an interlayered organic phase. (C) As-designed scaffolds inspired by nacre.

2.3 Fabrication of bioinspired composites

Bioinspired zirconia/PMMA composites were fabricated via 3D printing and polymer infiltration, as schematically illustrated in **Fig. 2**. Initially, as-sintered zirconia scaffolds were cleaned in an ethanol bath and then hydroxylated in piranha solution (75 vol.% H_2SO_4, 25 vol.% H_2O_2) for 30 min at room temperature in order to promote chemically bonding with silane coupling agent (γ-MPS). Subsequently, the scaffolds were surface-grafted with γ-MPS. The end groups of the silane coupling agent, the organofunctional and the alkoxy group, can form strong bonds with the polymer matrix and with the ceramics, therefore enhancing the interfacial bonding between the zirconia scaffold and poly (methyl methacylate) (PMMA) [17]. This involved soaking the hydroxylated scaffolds for up to 24 h in a mixed solution of 50 vol.% γ-MPS and 50 vol.% acetone.

The as-grafted scaffolds were then rinsed with acetone to remove the residual silane coupling agent and finally dried at room temperature for 12 h.

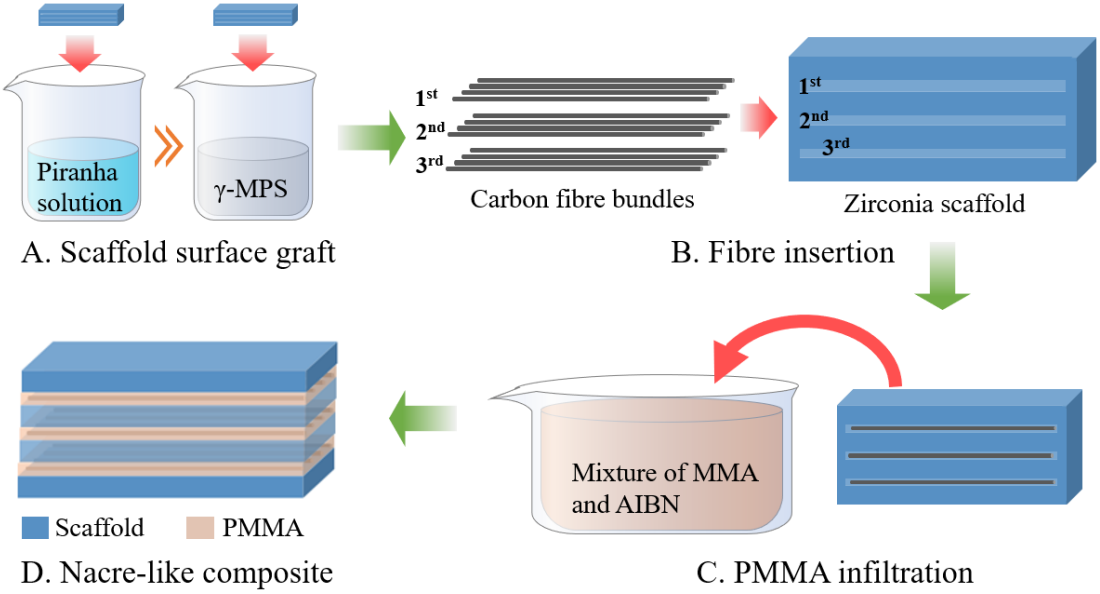

Fig. 2. Schematic illustration of the fabrication process of the layered composites. (A) Surface graft of the zirconia scaffold. (B) Fibre bundles were inserted into the gap of the scaffold. (C) The scaffold with fibre was immersed into a plastic mould for *in-situ* polymerization of MMA. (D) A nacre-like ZrO_2/cPMMA composite was finally obtained after polishing. The formation of ZrO_2/PMMA composite followed the same process except for the embedding step of the carbon fibre bundles. See the Supporting Information for full details.

Single-layered carbon fibre bundles (**Fig. S4**, Supporting information) were cut into several pieces with an area of 22 × 3 mm^2 each. After cleaning with ethanol and drying at room temperature, they were inserted into the gaps of the scaffolds for subsequent polymer infiltration (see **Fig. S5**, Supporting information). In the latter step, the treated scaffolds with and without embedded carbon fibre bundles were placed into a glass container that have already contained a mixture of MMA and AIBN in a weight ratio of 1:0.005 at room temperature. The container was then placed at 80°C in an oil bath for 20 min in order to activate the radical polymerization of the MMA. Then the container was left in an oven at 45°C overnight prior to post curing at 100°C for 2 h to ensure

complete polymerization. Prior to mechanical testing, the resulting composites were polished with SiC sandpaper of grade 600 to remove any excess polymer using a rotating polishing machine (LaboPol-5, Struers, Copenhagen, Denmark).

The resulting ternary bioinspired zirconia/carbon fibre/PMMA composites made of 60, 65, 70 and 75 vol.% of zirconia scaffolds are referred to as $ZrO_2$60/cPMMA, $ZrO_2$65/cPMMA, $ZrO_2$70/cPMMA and $ZrO_2$75/cPMMA, whilst the binary ZrO_2/PMMA composites are referred to $ZrO_2$60/PMMA, $ZrO_2$65/PMMA, $ZrO_2$70/PMMA and $ZrO_2$75/PMMA.

2.4 Microstructural characterisation

All microstructures of the parts were imaged by scanning electron microscopy (SEM, ZEISS Merlin, Oberkochen, Germany) at an accelerating voltage of 5 kV at a working distance of 8 mm, prior to SEM observation, all parts were polished to a 1 μm finish using the same polishing machine, the samples were then sputter-coated with a layer of Pt at a current of 10 mA for 5 min. ImageJ software was conducted to measure the thickness of the ceramic and the polymer lamellae as well as the diameters of the carbon fibres on SEM image.

2.5 Mechanical characterisation

Three-point flexural strength testing was undertaken on unnotched beams with a span of 20 mm at a crosshead displacement speed of 0.5 mm/min followed the test standard of ASTM C1161-13. The bending stress-strain curves were obtained from the load-displacement data according to the Euler-Bernoulli bending theory [18]:

$$\sigma = \frac{3FS}{2BW^2} \quad (1)$$

$$\varepsilon = \frac{6DW}{S^2} \quad (2)$$

where σ and ε are respectively the bending stress and strain, F is the force, S is the support span, B is the width of the specimen, W is the height of the specimens and D is the bending displacement at the middle point.

The single-edge V-notched beam (SEVNB) method was used to determine the fracture toughness of the composites, with a loading rate of 0.1 mm/min following ASTM standard C1421-99. The 3 mm wide SEVNB specimens were polished to a 1 μm finish using silicon carbide paper and then notched at one edge with a low-speed diamond saw of 200 μm thickness. The bottom of each notch was sharpened by repeatedly passing a razor blade with diamond paste to obtain a small sized pre-crack. The measurement of the notch depth was conducted using an optical microscope (Axio Observer 3, Zeiss, Germany); a typical notch is shown in **Fig. 3**, the notch depth to sample height ratio was maintained at 0.4 – 0.6 to ensure an accurate fracture toughness value [19]. The fracture toughness (K_{IC}) was calculated using the following equation:

$$K_{IC} = \frac{3PS}{2BW^{1.5}} \times \left(\frac{a}{W}\right)^{0.5} \times \frac{1.99 - \frac{a}{W} \times \left(1 - \frac{a}{W}\right)\left(2.15 - 3.93\frac{a}{W} + 2.7\left(\frac{a}{W}\right)^2\right)}{\left(1 + 2\frac{a}{W}\right)\left(1 - \frac{a}{W}\right)^{1.5}} \quad (3)$$

where P is the applied load, a is the notch depth. The fracture toughness of the monolithic zirconia was obtained from our previous work [20]. The work of fracture reveals how much energy is dissipated during bending fracture process [21][22]. It was calculated by dividing the area under the load displacement curve of the notched bars

over the specimen cross-section area, equation (4):

$$W_f = \frac{A}{2B(W-a)} \tag{4}$$

where W_f is the work of fracture (J/m^2), A is the total area under the load displacement curve and indicates the energy of the applied load during the fracture test, B and W are the width (m) and height (m) of the SEVNB specimen and a is the initial notch depth (m). For each test, at least 5 samples were tested to obtain an average value. All the mechanical property measurements were conducted using a universal testing machine (LABSANS, Shenzhen, China) with a 3 kN load cell.

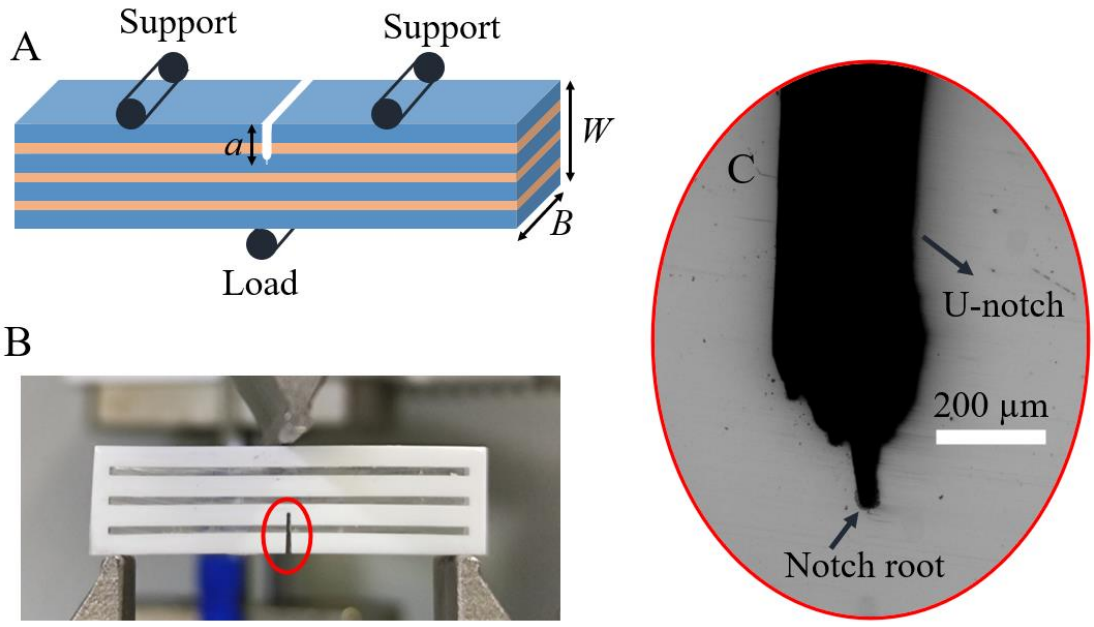

Fig. 3. Schematic diagram of SEVNB specimens and testing configuration. (A) Illustration of a fracture toughness test specimen. (B) SEVNB testing setup configuration. (C) Optical micrograph of a typical pre-crack notch with a root radius of ~15 μm.

3. Results and Discussion

3.1 Microstructure

The microstructures of the nacre-like composites are illustrated by a $ZrO_2$65/PMMA

composite with and without a surface grafted scaffold, **Fig. 4**. It is clear from the SEM images that the composites exhibited uniform polymer and ceramic lamellas and that the lamellae thickness was very close to that of the designed value; this suggests that DLP printing can achieve highly dimensional accuracy. Moreover, **Fig. 4A** demonstrates the absence of obvious structural flaws, such as pores and microcracks. Microstructural observations at the inorganic/organic phase interface revealed good adhesion in **Fig. 4B**, thanks to the chemical grafting at the molecular level before PMMA infiltration using *in-situ* free-radical polymerization, the presence of methacrylate groups acting to promote stronger covalent bonding between the inorganic and organic phase. However, obvious delamination can be observed at the non-grafted two-phase interface, **Fig. 4D**, which is not helpful to achieving good mechanical properties for the composites. The fabrication of excellent composites requires several key factors, including a suitable zirconia suspension, optimised printing parameters, a good debinding and sintering process, and successful surface grafts and polymer infiltration.

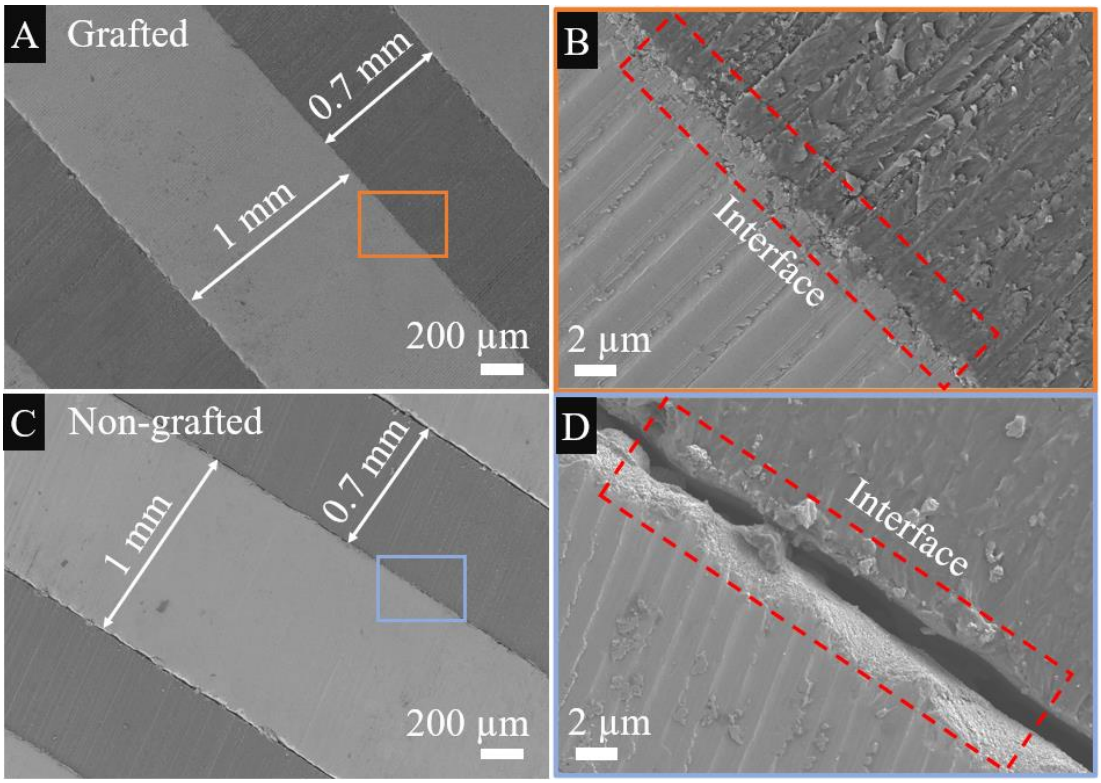

Fig. 4. Comparison of microstructure of the $ZrO_2$65/PMMA composites, containing 65 vol.% zirconia with 1 mm lamellae thickness and 35 vol.% 0.7 mm thickness PMMA lamellae. The lighter phase is the zirconia; the dark phase is the PMMA. (A & B) SEM micrographs of the composites with a surface grafted scaffold, (C & D) SEM micrographs of the composite without a surface grafted scaffold; delamination was observed at the inorganic/organic layer interfaces.

Fig. 5 shows the microstructures of the carbon fibre bundles and cross-section of the composites; the arrangement of the former was observed before the composites were produced. Clearly, they have a continuous and uniform features with a 7 µm diameter. As shown in **Fig. 5C**, the carbon fibres were uniformly dispersed in the polymer matrix without obvious agglomeration. The calculated volume fraction in the zirconia/cPMMA composite was ~15% and it can be seen that the volume fraction of the fibres played a significant role in the determination of the composite's mechanical strength. Thought it has been observed in the past that higher fibre volume fractions do not always lead to superior mechanical properties [23][24]. Actually, an excessive number of fibres in the

matrix may result in insufficient infiltration of the matrix, yielding voids and defects that are not beneficial for strong interfacial bonding. The presence of the latter can be observed in **Fig. 5D**; a large amount of polymer matrix covers the fibre surface. Appropriate interfacial bonding is important, as it can trigger toughening mechanisms such as fibre 'pull-out' and interfacial debonding, which consume significant amounts of fracture energy, further improving the properties of the composites [25]. Having an interfacial bond that is too strong or too weak can result in difficulties in inducing the desired toughening mechanisms [26].

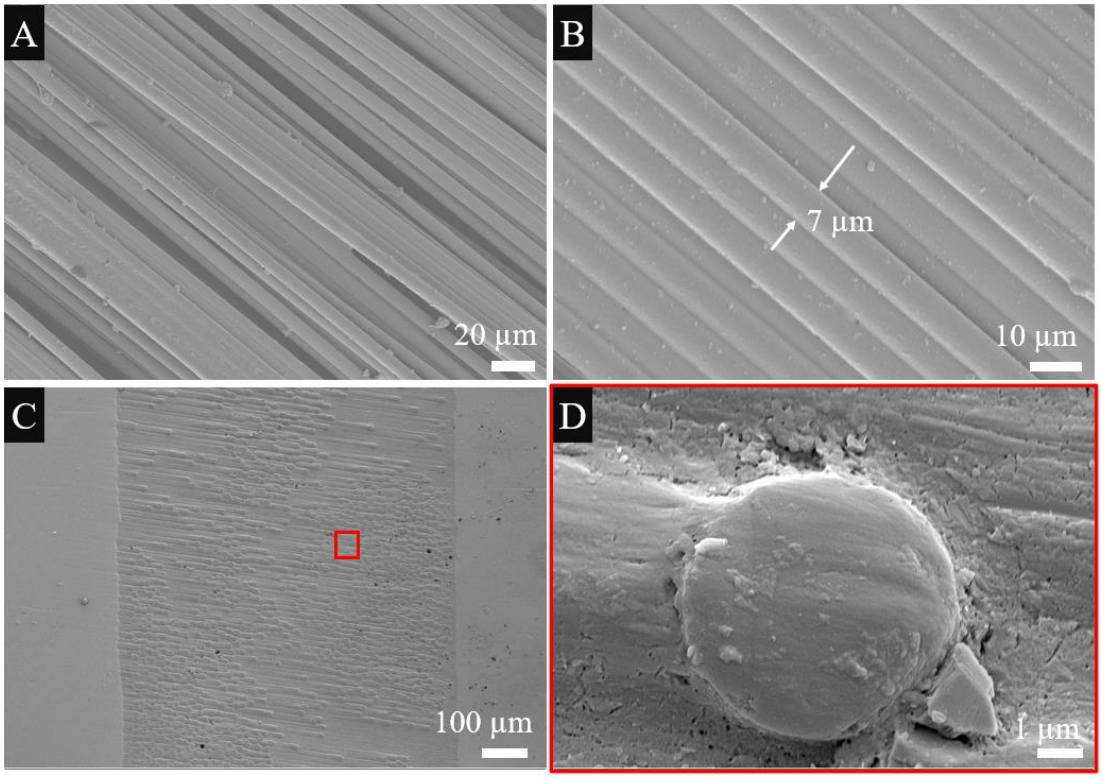

Fig. 5. SEM images of carbon fibre bundles and composites. (A) Carbon fibre bundles used in this study. (B) The magnified image of the carbon fibre bundle having a diameter of 7 µm. (C) Carbon fibres in the composites. (D) SEM observation showing strong interfacial bonding between polymer and fibre.

3.2 Mechanical properties

Fig. 6 shows the typical stress-strain curves of the $ZrO_2$75/PMMA and $ZrO_2$75/cPMMA composites, together with a stress-strain curve for 3D printed monolithic zirconia for comparison. The composites exhibited non-brittle failure due to the plastic deformation of the polymer phase, whilst the monolithic zirconia fractured catastrophically, though, as expected, it had a higher failure stress. Moreover, it can be seen that the areas under the stress-strain curves for the composites were larger than that of the monolithic zirconia; this suggests they had an improved fracture toughness and work of fracture. Typically, the composites had a step-like fracture mode, which is a typical response characteristic of a brittle/ductile alternative layered composites [27]; such behaviour is also found in ceramic/metal composites [28]. The $ZrO_2$75/PMMA and $ZrO_2$75/cPMMA composites were comprised of four-layers of ceramic lamellae and three-layers of polymer phase, and the steps in the stress-strain curve are believed to relate to the failures in the layers. The stress initially dropped dramatically, which corresponded with the crack propagating through the first zirconia layer and then rose again, representing crack accumulation inside the brittle layers after deflection. This process was repeated three times until the specimens failed completely. The step-like curve reveals that the ceramic/polymer interface prevented further crack propagation and caused the crack to deflect, thus a higher load (i.e. more energy) was needed for failure. Moreover, the $ZrO_2$75/cPMMA composites demonstrated a higher stress at the same loading strain compared to the $ZrO_2$75/PMMA composite materials. This was due to the introduction of fibres into polymer phase, in which fibre ‘pull-out’ has been witnessed in terms of its success in fibre-reinforced polymer composites [29][30][31].

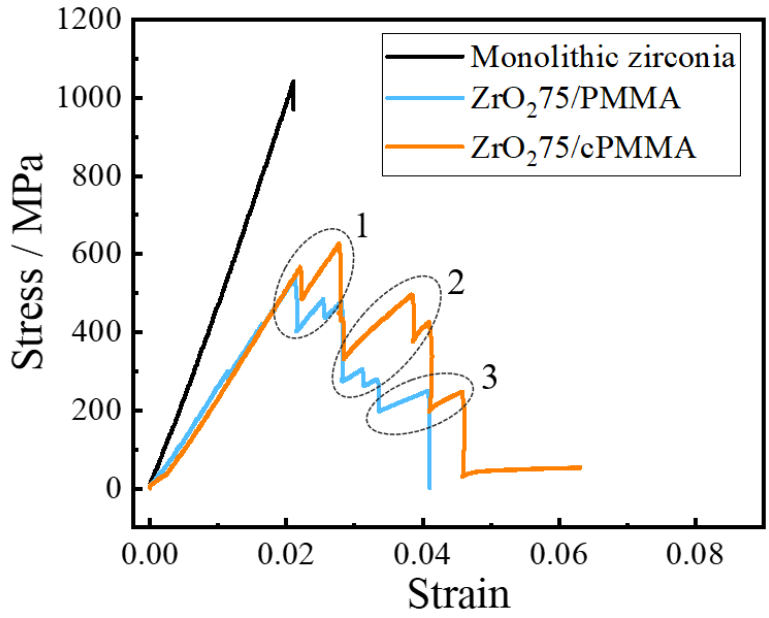

Fig. 6. Representative bending stress-strain curves of monolithic zirconia and bioinspired composites with 75 vol.% ceramic content.

Three-point bending tests were conducted to determine the flexural strength of the monolithic zirconia and its composites. **Fig. 7** shows a comparison of the flexural strength for the ZrO_2/PMMA and ZrO_2/cPMMA composites with varied ceramic content. It is interesting to observe that the flexural strength of the composites was strongly dependent on both the ceramic content and presence of the carbon fibres. With respect to the latter, the composites containing carbon fibres were always stronger than their fibre-less counterparts, on average by 12.6%, whilst the strength also increased by >200 MPa as the ceramic content increased from 60% to 75%, both with and without the carbon fibres. The improvement in the flexural strength in the carbon fibre-based composites compared to the fibre-free composites can be attributed to the significant amount of fibre 'pull-out'. This 'pull-out' of the fibres in the polymer matrix will have enhanced the strength of matrix and hence further improved the strength of composites.

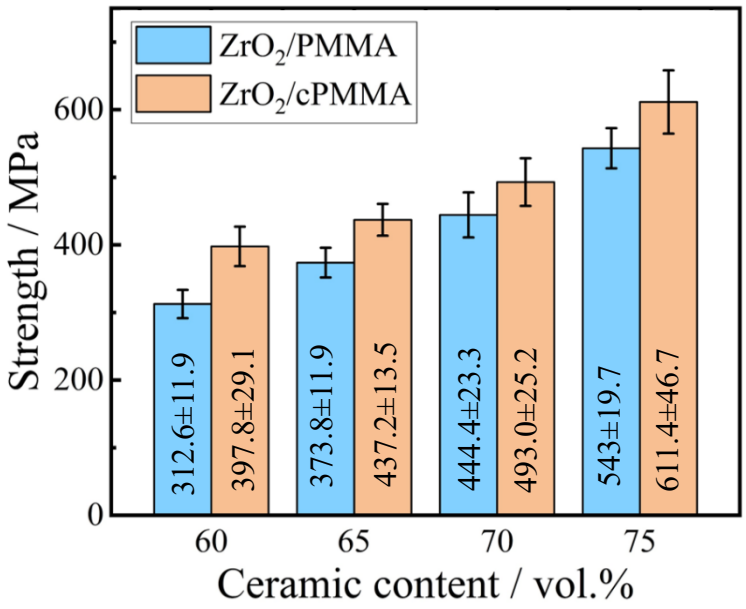

Fig. 7. The flexural strength of composites as a function of ceramic content.

Fig. 8 shows the fracture toughness and work of fracture as a function of ceramic content. Similar to the variation in strength, **Fig. 7**, the fracture toughness and work of fracture also demonstrated a strong dependence on both the ceramic content and presence of the carbon fibres. In all cases, both the fracture toughness and work of fracture were enhanced by the presence of the latter, the values increasing by an average of 74.5% and 125.4% respectively. Similarly, for the composites without carbon fibres the fracture toughness increased by 125.7% from 6.08 ± 0.54 to 13.72 ± 0.95 MPa $m^{1/2}$ as the ceramic content increased from 60 to 75 vol.%, whilst the work of fracture approximated doubled from 2125.1 ± 91.9 to 5863.8 ± 77.4 J/m^2. For the composites containing carbon fibres, whilst the magnitude of the increases was smaller, as indicated, the absolute values were somewhat higher as shown on **Fig. 8**. It can clearly be concluded that the results of the mechanical property measurements demonstrated the benefits of increasing the ceramic content and adding continuous carbon fibres.

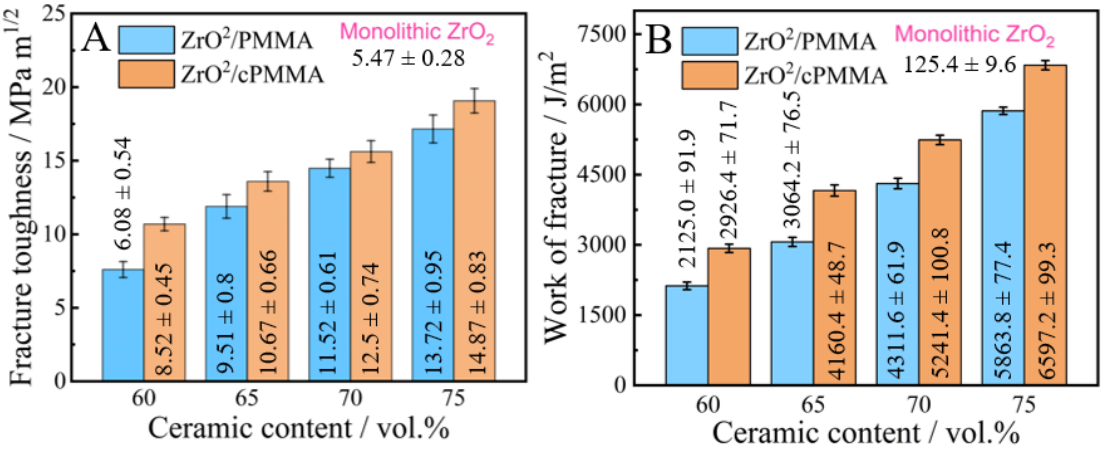

Fig. 8. Mechanical properties of the layered composites as a function of ceramic content. (A) Fracture toughness of the composites as compared to monolithic ZrO_2. (B) Work of fracture of the composites as compared to monolithic ZrO_2.

Fig. 8 also shows a comparison of the composites' and monolithic zirconia ceramics' values for both fracture toughness and work of fracture; it can be seen how they were both very significantly improved, particularly for the work of fracture. The latter revealing how the composites dissipated considerably more energy during the fracture process. Similarly, the load-displacement curves for the SEVNB tests yielded maximum load and displacement values of 71 N and 0.049 mm for the monolithic ZrO_2, whilst they were 584 N and 0.43 mm for $ZrO_2$75/cPMMA composites, respectively.

Fig. 9 provides a property map for the different composites without the presence of carbon fibres, together with schematic illustrations of the architecture of the different layered composites to help visualise the trends in the mechanical properties. As indicated earlier, both the fracture toughness and flexural strength of the composites show a clear trend with respect to the fraction of the ceramic in the ZrO_2/PMMA composites, becoming both stronger and tougher. These results suggest that the main contribution to the strength and fracture toughness of composites is the presence of the

thick ceramic lamellae that resisted fracture, whilst the polymer layer between the lamellae behaved like the ductile phase in nacre, dissipating fracture energy [6].

The mechanical properties of the bioinspired composite materials were strongly dependent on the layer thickness ratio, (t_c/t_p), where t_c and t_p represent the thickness of the ceramic and polymer layers, respectively [32]. Whilst a high ceramic content typically results in a greater layer thickness ratio, which yields outstanding mechanical properties, a very thin polymer layer thickness means the composition of the composites mainly consists of ceramic phase, which maximises strength but minimises fracture toughness. Therefore, it may be concluded that there will be an optimal ceramic content or layer thickness ratio to achieve the best combination of toughness and strength as predicted by Magrini et al [33] and Wan et al [34]. Magrini et al evaluated the flexural strength for nacre-like alumina/PMMA composites with ceramic contents in the range 35-59 vol.% whilst Wan et al undertook a very similar activity for composites containing 50-85 vol.% of ceramic phase. Both concluded that whilst a higher ceramic content generally resulted in improvement in both strength and fracture toughness, there would be a threshold, above which the composites would exhibit a brittle failure response and hence a low fracture toughness. This was determined to be a ceramic content of >85 vol.% by Wan et al.

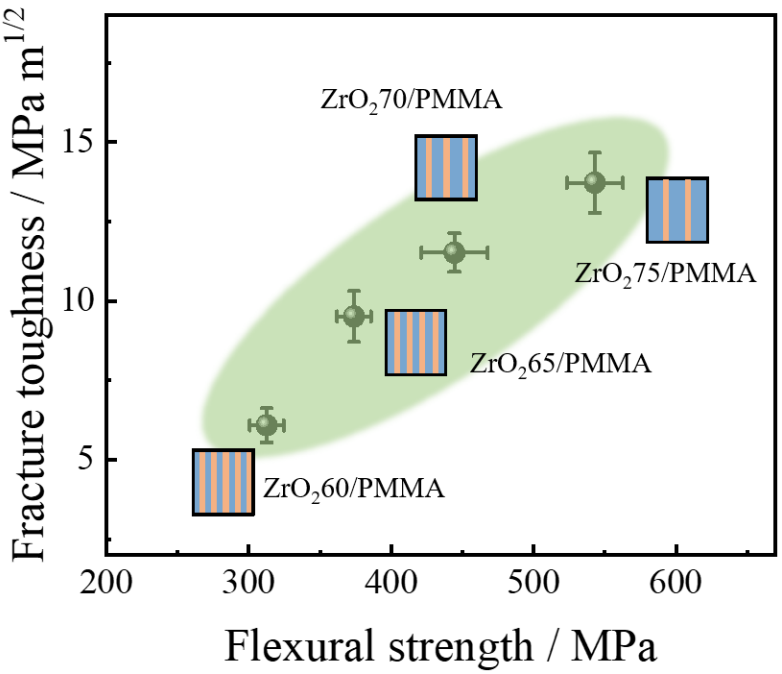

Fig. 9. Property map of ZrO_2/PMMA composites as a function of ceramic content. A schematic of the architecture of each group of composites is depicted, in which the ceramic layer is represented in blue and the polymer in orange. Both fracture toughness and flexural strength are proportional to the ceramic content in the range 60-75 vol.%.

3.3 Toughening mechanism of composites

The excellent mechanical properties of the nacre-like composites are largely associated with both intrinsic and extrinsic toughening mechanisms [32]. The former is derived from the extensive inelastic deformation of PMMA, which increases the inherent resistance to crack initiation and propagation, whilst the later can be attributed to the layered architecture, fibre 'pull-out' and fibre debonding, which inhibits crack growth by effectively reducing the crack-driving force.

Fig. 10 presents the crack propagation pattern of the composites during the fracture process. As can be seen, the crack was preferentially initiated in the brittle ceramic layer and then it propagated through it until it met the ceramic-polymer interface, where it

would propagate along the strong ceramic-polymer interface, leading to interfacial debonding, **Fig. 10B**, and an increase in the composite's toughness. It is believed that the strong interfacial bonding resulting from the chemical grafting promoted multiple extrinsic toughening mechanisms that stabilised the crack growth avoiding the catastrophic fracture that is characteristic of monolithic zirconia. The ligament polymeric phase deflects the cracks and releases the stress at the crack tip by a mechanism known as "crack-tip-shielding" [35], which provides a means of blunting the crack tip. Such crack blunting has been identified as an important toughening mechanism that acts to lower crack-tip stresses [36]. Maximilien et al [32] further concluded that an increased polymer layer thickness could increase the degree of blunting. Alternating brittle–ductile layered composites thus lead to extensive crack deflections, corresponding to tortuous zig-zag crack paths. The damage results in the nucleation of a number of microcracks formed in the polymer phase ahead of the propagating crack and inelastic deformation of the ductile layers undergoing extensive stretching, thereby acting as uncracked ligament bridges prior to failure, **Fig. 10D**. Additionally, the ceramic lamellae can exhibit a degree of 'pull-out', **Fig. 10C**, with significant shear deformation within the polymeric layers absorbing a large amount of fracture energy, both factors undoubtedly increased the fracture toughness of the composites.

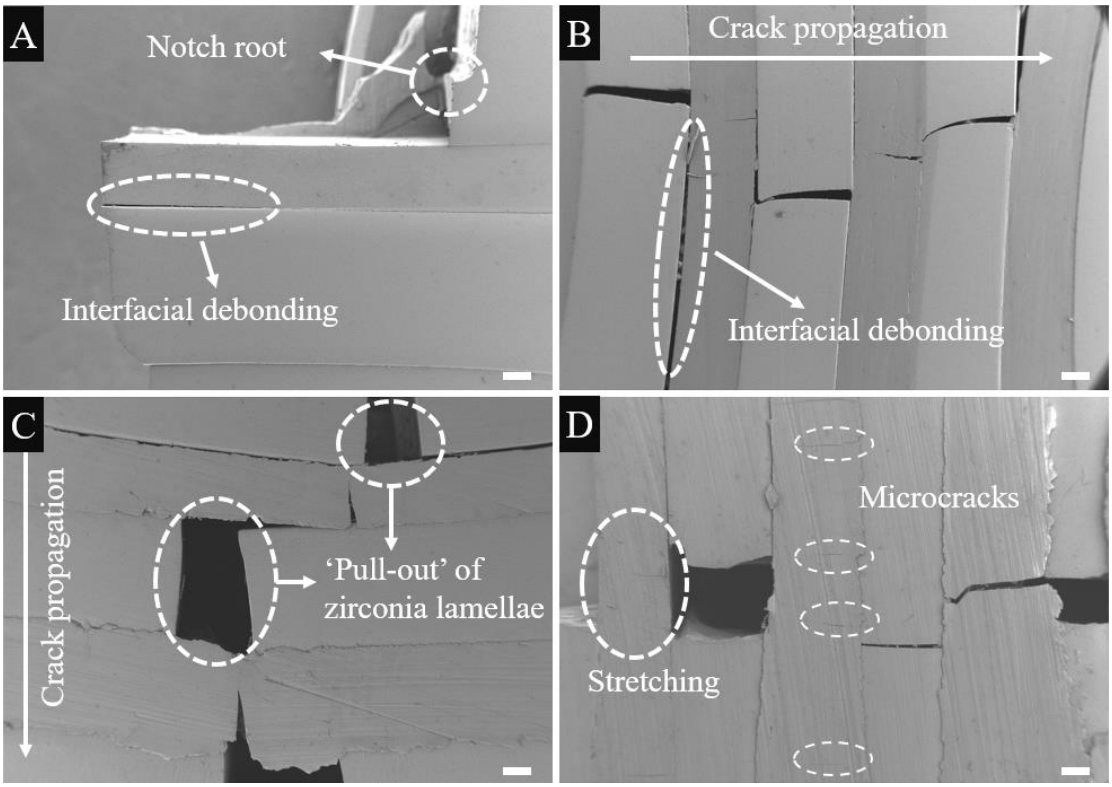

Fig. 10. Representative microstructures of crack propagation of the bioinspired layered composites. (A) Crack initiation at the root of the notch and its deflection after the interaction with the polymer layer. (B) Extensive interfacial debonding was observed during cracking. (C) 'Pull-out' of the ceramic lamellae causes significant tearing and stretching of the polymer layer. (D) The formation of microcracks in the polymer phase ahead of the crack tips could consume a large amount of energy. Scale bar: 200 μm.

Fig. 11 shows the representative fracture surface morphology of the $ZrO_2$70/cPMMA composite. It can be seen that the carbon fibre bundles were reasonably uniformly dispersed in the polymer layers, **Fig. 11A**, and the obvious brittle fracture of the ceramic phase and interphase delamination may be observed. Visible fibre 'pull-out' and fibre-polymer interfacial debonding are both observed in the fracture surface of the $ZrO_2$70/cPMMA composites, **Fig. 11B**, which corresponds to the additional toughening mechanism relative to reported bioinspired ceramic composites [37][38][39][40][41]. In addition, the fracture surface in the polymer matrix shows a step-like mode, this indicates crack deflections during growth. Meanwhile, the fibres will absorb more

energy before rupture [42]. The work of fracture of the $ZrO_2$70/cPMMA composites was 4311.6 ± 61.9 J/m^2; this increased by 22.5% to a value of 5241.4 ± 100.8 J/m^2 with the incorporation of carbon fibres into the PMMA phase. Similarly, the strength increased by 10.9% from 444.4 ± 23.3 MPa to 493 ± 25.2 MPa. It can therefore be seen that the toughening and strengthening effect from adding the carbon fibres was quite prominent. Observation of the fracture surface of the polymer phase also indicated that it exhibited a step-like morphology and extensive inelastic deformation, **Fig. 11C**, which will have contributed to the high toughness of the composites. The 'pull-out' of the carbon fibres and the debonded interfaces can also be clearly observed in **Fig. 11D,** which means that more fracture energy was consumed during the fracture process, as indicated by its improved fracture toughness and work of fracture.

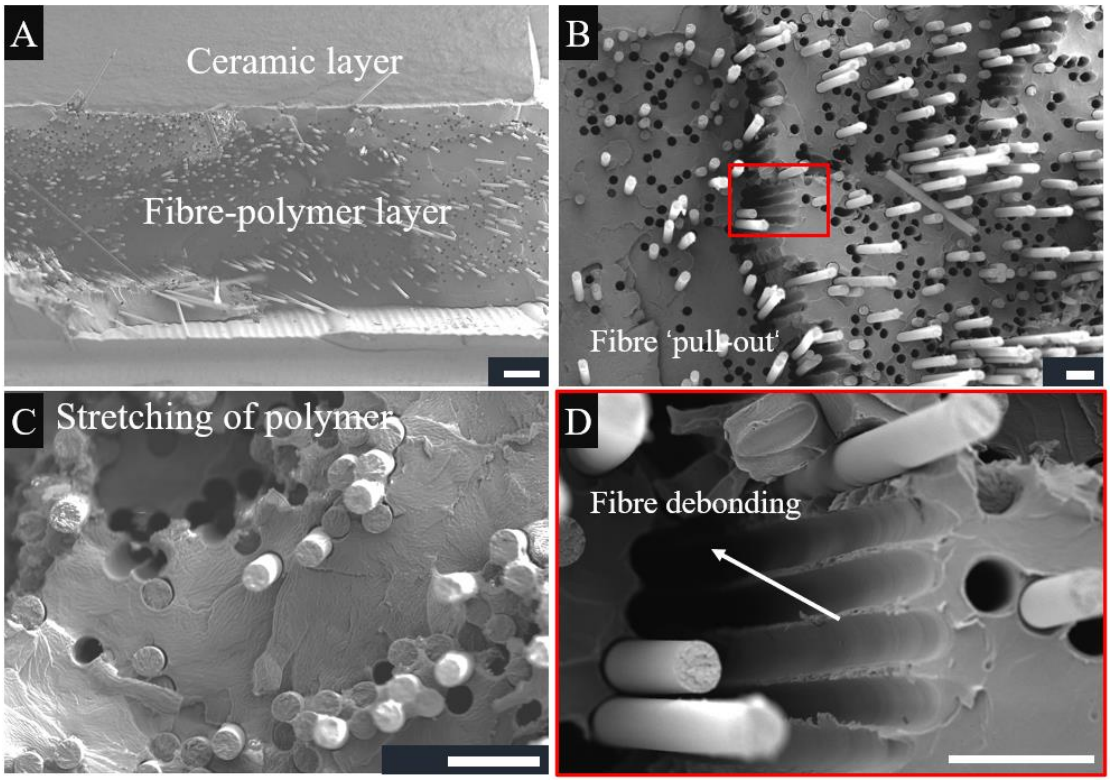

Fig. 11. Representative microstructures of the fracture surface in ZrO_2/cPMMA

composites. (A) Cross-section of the fracture morphology representing the uniformly dispersed carbon fibres in the PMMA layer (scale bar: 100 μm). (B) SEM image illustrating the extensive fibre 'pull-out' and crack deflection. (C) Stretching of the polymer phase. (D) Observation of fibre debonding. (B, C, and D scale bar: 20 μm).

3.4 Comparison to other bioinspired layered ceramic composites

Fig. 12 shows a direct comparison of the mechanical properties of the bioinspired layered composites with those of other bioinspired composites. It can be clearly seen that the $ZrO_2$75/cPMMA composites display a remarkable combination of strength (611.4 MPa), fracture toughness (14.87 MPa $m^{1/2}$) and work of fracture (6597.2 J/m^2). With respect to the flexural strength and fracture toughness of the resulting composites, they are greater than those of other reported bioinspired composites based on zirconia, alumina or silica carbide and containing either an organic, metallic, or ceramic phase. This can be attributed to the addition of the carbon fibre bundles into the polymer layer, which introduced the additional toughening mechanism of fibre 'pull-out'. Moreover, the composites also outperformed the work of fracture for the other composites, as shown in **Fig. 12B** and had a work of fracture value almost 50 times higher than for monolithic zirconia. A significant improvement in toughness of $ZrO_2$75/cPMMA composites was witnessed due to the extensive toughening mechanism introduced by the brick-and-mortar architecture.

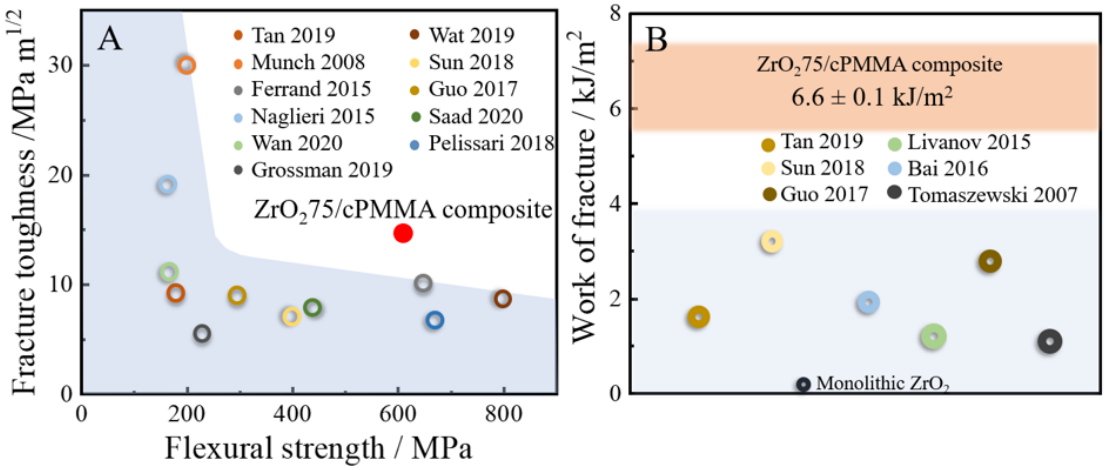

Fig. 12. Comparison of the layered composites with other bioinspired composites. (A) Strength and fracture toughness [43][14][44][6][34][45][40][35][46][47][48]. (B) Work of fracture [13][18][27].

4. Conclusions

Nacre-like ZrO_2/PMMA and ZrO_2/cPMMA composites were successfully fabricated via 3D printing followed by an in-situ polymerization of the MMA. The resulting composites with the "brick-and-mortar" architecture exhibited the ability to be damage-tolerant combined with non-catastrophic failure. A variety of toughening mechanisms were identified, including the 'pull-out' of carbon fibres and ceramic lamellae, fibre-polymer, and ceramic-polymer interfacial debonding, crack deflection and inelastic deformation of polymeric layers. These toughening mechanisms can dissipate large amounts of energy, thereby leading to an excellent combination of strength and toughness. The mechanical properties were investigated and the results can be summarized as:

1. The mechanical properties of composites were strongly dependent on ceramic content. Specifically, flexural strength, fracture toughness and work of fracture

displayed a significant increase with increasing ceramic volume fraction.

2. The mechanical properties of all of the ZrO_2/cPMMA composites were somewhat higher than those of the equivalent ZrO_2/PMMA composites, thanks to the addition of carbon fiber in the polymer matrix, which acted as an effective strengthening and toughening method.
3. An excellent combination of high strength (611.4 ± 46.7 MPa), fracture toughness (14.87 ± 0.83 MPa $m^{1/2}$) and work of fracture (6597.2 ± 99.3 J/m^2) was achieved in the $ZrO_2$75/cPMMA composites as the ceramic content reached 75 vol.%. The fracture toughness and work of fracture were, respectively, ~2.7 and ~50 times higher than those of monolithic zirconia, respectively.
4. Compared to monolithic zirconia and other bioinspired ceramic/compliant phase composites, the mechanical properties of the resulting $ZrO_2$75/cPMMA composites with lamellar architectures are extremely competitive.

Declaration of competing interest

The authors declare that they have no known competing financial interests or personal relationships that could have influenced the work reported in this paper.

Acknowledgement

The authors acknowledge the assistance of SUSTech Core Research Facilities. This work was financially supported by Guangdong Province International Collaboration

Programme [Grant no. 2019A050510003] and Shenzhen Key Laboratory for Additive Manufacturing of High-performance Materials [Grant no. ZDSYS201703031748354].

References:

[1] W. D. Kingery, H. K. Bowen, D. R. Uhlmann, R. Frieser, "Introduction to Ceramics," *J. Electrochem. Soc.*, 1977, doi: 10.1149/1.2133296.

[2] J. Rösler, M. Bäker, H. Harders, "Mechanical behaviour of ceramics," in *Mechanical Behaviour of Engineering Materials*, 2007.

[3] S. Askarinejad, N. Rahbar, "Toughening mechanisms in bioinspired multilayered materials," *J. R. Soc. Interface*, 2015, doi: 10.1098/rsif.2014.0855.

[4] H. Kakisawa, T. Sumitomo, "The toughening mechanism of nacre and structural materials inspired by nacre," *Sci. Technol. Adv. Mater.*, 2011, doi: 10.1088/1468-6996/12/6/064710.

[5] S. Deville, E. Saiz, R. K. Nalla, A. P. Tomsia, "Freezing as a path to build complex composites," *Science (80-.).*, 2006, doi: 10.1126/science.1120937.

[6] V. Naglieri, B. Gludovatz, A. P. Tomsia, R. O. Ritchie, "Developing strength and toughness in bio-inspired silicon carbide hybrid materials containing a compliant phase," *Acta Mater.*, 2015, doi: 10.1016/j.actamat.2015.07.022.

[7] M. Sarikaya, K. E. Gunnison, M. Yasrebi, I. A. Aksay, "Mechanical Property-Microstructural Relationships in Abalone Shell," *MRS Proc.*, 1989, doi: 10.1557/proc-174-109.

[8] J. Sun, B. Bhushan, "Hierarchical structure and mechanical properties of nacre: A review," *RSC Advances*. 2012, doi: 10.1039/c2ra20218b.

[9] H. Hadraba, D. Drdlik, Z. Chlup, K. Maca, I. Dlouhy, J. Cihlar, "Layered ceramic composites via control of electrophoretic deposition kinetics," *J. Eur. Ceram. Soc.*, 2013, doi: 10.1016/j.jeurceramsoc.2013.01.026.

[10] G. E. Stan, D. Bojin, "Adherent glass-ceramic thin layers with bioactive potential deposited by magnetron sputtering techniques," *UPB Sci. Bull. Ser. B Chem. Mater. Sci.*, 2010.

[11] R. Roy, S. Komarneni, D. M. Roy, "Multi-Phasic Ceramic Composites made by Sol-Gel Technique," *MRS Proc.*, 1984, doi: 10.1557/proc-32-347.

[12] Q. Cheng, C. Huang, A. P. Tomsia, "Freeze Casting for Assembling Bioinspired Structural Materials," *Adv. Mater.*, 2017, doi: 10.1002/adma.201703155.

[13] H. Bai, F. Walsh, B. Gludovatz, B. Delattre, C. Huang, Y. Chen, A. P. Tomsia, R. O. Ritchie, "Bioinspired Hydroxyapatite/Poly(methyl methacrylate) Composite with a Nacre-Mimetic Architecture by a Bidirectional Freezing Method," *Adv. Mater.*, 2016, doi: 10.1002/adma.201504313.

[14] E. Munch, M. E. Launey, D. H. Alsem, E. Saiz, A. P. Tomsia, R. O. Ritchie, "Tough, bio-inspired hybrid materials," *Science (80-.).*, 2008, doi: 10.1126/science.1164865.

[15] H. Zhao, L. Guo, “Nacre-Inspired Structural Composites: Performance-Enhancement Strategy and Perspective,” *Adv. Mater.*, 2017, doi: 10.1002/adma.201702903.

[16] Z. C. Eckel, C. Zhou, J. H. Martin, A. J. Jacobsen, W. B. Carter, T. A. Schaedler, “Additive manufacturing of polymer-derived ceramics,” *Science (80-.).*, 2016, doi: 10.1126/science.aad2688.

[17] Y. Xie, C. A. S. Hill, Z. Xiao, H. Militz, C. Mai, “Silane coupling agents used for natural fiber/polymer composites: A review,” *Compos. Part A Appl. Sci. Manuf.*, vol. 41, no. 7, pp. 806–819, 2010, doi: 10.1016/j.compositesa.2010.03.005.

[18] E. Pogorelov, K. Tushtev, A. Arnebold, K. Koschek, A. Hartwig, K. Rezwan, “Strong and super tough: Layered ceramic-polymer composites with bio-inspired morphology,” *J. Am. Ceram. Soc.*, 2018, doi: 10.1111/jace.15717.

[19] W. Zhao, C. Peng, M. Lv, M. Bai, P. Rao, “Effect of notch depth on fracture toughness of Y-TZP and determination of its actual value,” *Ceram. Int.*, 2015, doi: 10.1016/j.ceramint.2014.08.130.

[20] J. Sun, X. Chen, J. Wade-Zhu, J. Binner, J. Bai, “A comprehensive study of dense zirconia components fabricated by additive manufacturing,” *Addit. Manuf.*, vol. 43, no. April, p. 101994, 2021, doi: 10.1016/j.addma.2021.101994.

[21] H. G. Tattersall, G. Tappin, “The work of fracture and its measurement in metals, ceramics and other materials,” *J. Mater. Sci.*, 1966, doi: 10.1007/BF00550177.

[22] S. M. Barinov, M. Sakai, “The work-of-fracture of brittle materials: Principle, determination, and applications,” *J. Mater. Res.*, 1994, doi: 10.1557/JMR.1994.1412.

[23] M. El Messiry, “Theoretical analysis of natural fiber volume fraction of reinforced composites,” *Alexandria Eng. J.*, 2013, doi: 10.1016/j.aej.2013.01.006.

[24] A. M. Radzi, S. M. Sapuan, M. Jawaid, M. R. Mansor, “Influence of fibre contents on mechanical and thermal properties of roselle fibre reinforced polyurethane composites,” *Fibers Polym.*, 2017, doi: 10.1007/s12221-017-7311-8.

[25] H. He, J. Wang, K. Li, J. Wang, J. Gu, “Mixed resin and carbon fibres surface treatment for preparation of carbon fibres composites with good interfacial bonding strength,” *Mater. Des.*, 2010, doi: 10.1016/j.matdes.2010.05.031.

[26] Y. Zu, J. Sha, J. Li, Z. Zhang, S. Wang, Z. Lv, J. Dai, “Effect of multi-walled carbon nanotubes on microstructure and fracture properties of carbon fiber-reinforced ZrB2-based ceramic composite,” *Ceram. Int.*, 2017, doi: 10.1016/j.ceramint.2017.03.018.

[27] K. Livanov, H. Jelitto, B. Bar-On, K. Schulte, G. A. Schneider, D. H. Wagner, “Tough alumina/polymer layered composites with high ceramic content,” *J. Am. Ceram. Soc.*, vol. 98, no. 4, pp. 1285–1291, 2015, doi: 10.1111/jace.13413.

[28] Y. Cao, C. Guo, S. Zhu, N. Wei, R. A. Javed, F. Jiang, “Fracture behavior of Ti/Al3Ti metal-intermetallic laminate (MIL) composite under dynamic loading,” *Mater. Sci. Eng. A*, 2015, doi: 10.1016/j.msea.2015.04.025.

[29] H. Fang, Y. Bai, W. Liu, Y. Qi, J. Wang, “Connections and structural applications of fibre reinforced polymer composites for civil infrastructure in aggressive environments,” *Composites Part B: Engineering*. 2019, doi: 10.1016/j.compositesb.2018.11.047.

[30] H. Zhang, D. Yang, Y. Sheng, “Performance-driven 3D printing of continuous curved carbon fibre reinforced polymer composites: A preliminary numerical study,” *Compos. Part B Eng.*, 2018, doi: 10.1016/j.compositesb.2018.06.017.

[31] R. R. Hughes, B. W. Drinkwater, R. A. Smith, “Characterisation of carbon fibre-reinforced polymer composites through radon-transform analysis of complex eddy-current data,” *Compos. Part B Eng.*, 2018, doi: 10.1016/j.compositesb.2018.05.007.

[32] M. E. Launey, E. Munch, D. H. Alsem, E. Saiz, A. P. Tomsia, R. O. Ritchie, “A novel biomimetic approach to the design of high-performance ceramic - Metal composites,” *J. R. Soc. Interface*, 2010, doi: 10.1098/rsif.2009.0331.

[33] T. Magrini, F. Bouville, A. Lauria, H. Le Ferrand, T. P. Niebel, A. R. Studart, “Transparent and tough bulk composites inspired by nacre,” *Nat. Commun.*, 2019, doi: 10.1038/s41467-019-10829-2.

[34] H. Wan, N. Leung, S. Algharaibeh, T. Sui, Q. Liu, H. Peng, B. Su, “Cost-effective fabrication of bio-inspired nacre-like composite materials with high strength and toughness,” *Compos. Part B Eng.*, 2020, doi: 10.1016/j.compositesb.2020.108414.

[35] M. Sun, Y. Bai, M. Li, S. Fan, L. Cheng, “Improved toughness and electromagnetic shielding-effectiveness for graphite-doped SiC ceramics with a net-like structure,” *J. Eur. Ceram. Soc.*, 2018, doi: 10.1016/j.jeurceramsoc.2018.08.038.

[36] M. Q. Sun, P. Shen, Q. C. Jiang, “Microstructures and mechanical characterizations of high-performance nacre-inspired Al/Al 2 O 3 composites,” *Compos. Part A Appl. Sci. Manuf.*, vol. 121, no. January, pp. 465–473, 2019, doi: 10.1016/j.compositesa.2019.04.007.

[37] F. Bouville, “Strong and tough nacre-like aluminas: Process-structure-performance relationships and position within the nacre-inspired composite landscape,” *Journal of Materials Research*. 2020, doi: 10.1557/jmr.2019.418.

[38] K. Radi, D. Jauffres, S. Deville, C. L. Martin, “Strength and toughness trade-off optimization of nacre-like ceramic composites,” *Compos. Part B Eng.*, 2020, doi: 10.1016/j.compositesb.2019.107699.

[39] R. Bermejo, “‘Toward seashells under stress’: Bioinspired concepts to design tough layered ceramic composites,” *J. Eur. Ceram. Soc.*, 2017, doi: 10.1016/j.jeurceramsoc.2017.04.041.

[40] A. Wat, J. I. Lee, C. W. Ryu, B. Gludovatz, J. Kim, A. P. Tomsia, T. Ishikawa, J. Schmitz, A. Meyer, M. Alfreder, D. Kiener, E. S. Park, R. O. Ritchie, “Bioinspired nacre-like alumina with a bulk-metallic glass-forming alloy as a compliant phase,” *Nat. Commun.*, 2019, doi: 10.1038/s41467-019-08753-6.

[41] U. G. K. Wegst, H. Bai, E. Saiz, A. P. Tomsia, R. O. Ritchie, “Bioinspired structural materials,” *Nat. Mater.*, 2015, doi: 10.1038/nmat4089.

[42] T. Liu, X. Tian, M. Zhang, D. Abliz, D. Li, G. Ziegmann, “Interfacial performance and fracture patterns of 3D printed continuous carbon fiber with sizing reinforced PA6 composites,” *Compos. Part A Appl. Sci. Manuf.*, 2018, doi: 10.1016/j.compositesa.2018.09.001.

[43] G. Tan, J. Zhang, L. Zheng, D. Jiao, Z. Liu, Z. Zhang, R. O. Ritchie, “Nature-Inspired Nacre-Like Composites Combining Human Tooth-Matching Elasticity and Hardness with Exceptional Damage Tolerance,” *Adv. Mater.*, 2019, doi: 10.1002/adma.201904603.

[44] H. Le Ferrand, F. Bouville, T. P. Niebel, A. R. Studart, “Magnetically assisted slip casting of bioinspired heterogeneous composites,” *Nat. Mater.*, 2015, doi: 10.1038/nmat4419.

[45] M. Grossman, D. Pivovarov, F. Bouville, C. Dransfeld, K. Masania, A. R. Studart, “Hierarchical Toughening of Nacre-Like Composites,” *Adv. Funct. Mater.*, 2019, doi: 10.1002/adfm.201806800.

[46] R. F. Guo, N. Guo, P. Shen, L. K. Yang, Q. C. Jiang, “Effects of ceramic lamellae compactness and interfacial reaction on the mechanical properties of nacre-inspired Al/Al2O3–ZrO2 composites,” *Mater. Sci. Eng. A*, vol. 718, no. November 2017, pp. 326–334, 2018, doi: 10.1016/j.msea.2018.01.088.

[47] H. Saad, K. Radi, T. Douillard, D. Jauffres, C. L. Martin, S. Meille, S. Deville, “A simple approach to bulk bioinspired tough ceramics,” *Materialia*, 2020, doi: 10.1016/j.mtla.2020.100807.

[48] P. I. B. G. B. Pelissari, F. Bouville, V. C. Pandolfelli, D. Carnelli, F. Giuliani, A. P. Luz, E. Saiz, A. R. Studart, “Nacre-like ceramic refractories for high temperature applications,” *J. Eur. Ceram. Soc.*, 2018, doi: 10.1016/j.jeurceramsoc.2017.10.042.